CCFE-PR(17)17

E. Havlickova, M. Wischmeier, B. Lipschultz, G. Fishpool

The Effect of the Super-X Divertor of MAST Upgrade on Impurity Radiation as Modelled by SOLPS

The Effect of the Super-X Divertor of MAST Upgrade on Impurity Radiation as Modelled by SOLPS

E. Havlickova[1], M. Wischmeier[2], B. Lipschultz[3], G. Fishpool[1]

[1]Culham Centre for Fusion Energy, Culham Science Centre, Abingdon, OX14 3DB, UK
[2]Max-Planck Institut f¨ur Plasmaphysik, Boltzmannstraße 2, D-85748 Garching, Germany
[3]Department of Physics, University of York, Heslington, York, YO10 5DD, United Kingdom

The effect of the Super-X divertor of MAST Upgrade on impurity radiation as modelled by SOLPS

E. Havlíčková[a,*], M. Wischmeier[b], B. Lipschultz[c], G. Fishpool[a]

[a] *Culham Centre for Fusion Energy, Culham Science Centre, Abingdon, OX14 3DB, United Kingdom*

[b] *Max-Planck Institut für Plasmaphysik, Boltzmannstraße 2, D-85748 Garching, Germany*

[c] *Department of Physics, University of York, Heslington, York, YO10 5DD, United Kingdom*

Abstract

An impurity seeding scan has been simulated in three different divertor configurations of MAST-U, showing the effect of the divertor geometry on the transition to detachment. The three configurations include a conventional short divertor, a Super-X divertor with large poloidal flux expansion and a Super-X divertor with small poloidal flux expansion. Both Super-X configurations detach at the same impurity seeding rate, while the detachment threshold in the conventional divertor is much higher. A comparison of SOLPS results for all configurations is presented in a detaching plasma with target temperatures around 5 eV. The total power balance, the distribution of radiation and the divertor closure with respect to neutrals and impurities is analyzed.

PACS: 52.55.Fa, 52.55.Rk, 52.65.Kj

PSI-21 keywords: Super-X divertor, detachment, impurity, radiation, edge modelling

[*] *Corresponding Author Address*: Culham Centre for Fusion Energy, Culham Science Centre, Abingdon, OX14 3DB, United Kingdom

[*] *Corresponding Author E-mail*: eva.havlickova@ccfe.ac.uk

Presenting Author: Eva Havlíčková

Presenting Author E-mail: eva.havlickova@ccfe.ac.uk

1. Introduction

Additional divertor design features beyond those planned for ITER might be necessary for a device like DEMO to achieve required heat handling performance and longevity. One of the concepts is the Super-X divertor (SXD) [1] which will be installed on the MAST-U tokamak [2, 3]. This novel configuration allows us to study the effect of the divertor magnetic topology on maximum radiation levels in the divertor and stability limits associated with radiation.

The new MAST-U divertor design allows us to vary the parallel length between the X-point and the target, poloidal magnetic flux expansion in the divertor and the strike point location. Such flexibility enables the effects of different parameters to be separated when studying the divertor performance and power exhaust issues. The MAST-U SXD has been extensively studied by simulation in [4, 5], from which this paper follows. The previous work discussed the potential of the SXD to increase power losses in the divertor, the divertor closure with respect to neutrals, and its potential to reduce divertor temperatures, target power loads and the density required for the transition to detachment.

For the purpose of this paper, a nitrogen seeding scan has been performed in three divertor configurations – a conventional divertor (CD) with the target closer to the X-point, smaller connection length and smaller magnetic flux expansion, a Super-X divertor with the target at larger radius, larger connection length and larger poloidal magnetic flux expansion (SXD1), and a long divertor with the target at larger radius, but smaller connection length and smaller poloidal magnetic flux expansion (SXD2). Nitrogen is puffed from a location inside the divertor away from the X-point, which allows a stable detachment in the simulation with a radiation zone inside the divertor leg. While here we focus on more detail comparison of the divertor configurations just at the detachment threshold of 5 eV, full scans will be described elsewhere [6] with less details devoted to a single comparison, but more attention given to maximizing

the radiated power fractions as well as to the stability of a radiating detached plasma in the simulation. All simulations have been performed in SOLPS5.0 with EIRENE without drifts and neutral-neutral collisions. Drift effects in MAST and MAST-U are studied elsewhere [7]. Neutral-neutral interactions are not expected to play a role in the studied MAST-U cases where neutral densities are below 1×10^{20} m^{-3}.

2. Nitrogen seeding scan and transition to detachment

Divertor configurations considered in this paper are shown in Fig. 1 and are up/down symmetric. The connection length between the midpalne and the target in the proximity of the separatrix is 20 m in the CD, 35 m in the SXD1 and 24 m in the SXD2. The total flux expansion (averaged over 5 mm of the radial distance at the outboard midplane) is 6 in the CD, 24 in the SXD1 and 14 in the SXD2. Note that the target design of the SXD in this paper is to allow a sensible like-with-like comparison with the CD and does not represent full range of capabilities of the machine which include both horizontal and vertical target conditions.

Nitrogen atoms are puffed from the divertor chamber as shown in Fig. 1. The starting point of each scan is a simulation of an H-mode plasma in MAST-U with narrow scrape-off layer (SOL), the input power $P_{\rm inp} = 1.7$ MW, the separatrix density $n_{\rm sep} \approx 1 \times 10^{19}$ m^{-3} and carbon as sputtered impurity. This case leads to higher temperatures in the SOL compared to a typical MAST experiment, but was chosen as an instructive case to show the transition to detachment in the two SXD configurations, as at lower power these configurations would be fully detached prior to impurity seeding. The fuelling source for deuterium is located at the core boundary of the grid. There is no pumping prescribed to the main chamber walls and the targets where the recycling coefficient is set to $R = 1$. Pumping occurs on cryopumps where $R = 0.9$ and which are located behind the outer targets. For more details see [4].

The magnetic geometry of the divertor clearly influences when the plasma detaches (Fig. 2).

The two SXD configurations need much smaller puffing rates for the particle flux to roll over (the temperatures are reduced already before the impurity puffing due to larger target radius and larger power losses [4]) and also the particle flux at the transition to detachment is smaller. In addition, the SXD configurations achieve a larger degree of detachment with a larger pressure drop along the field line as well as a sharper reduction of the target power load compared to the CD where the detachment is more gradual. The SXD2 detaches at the same puffing rate as the SXD1 as the target temperatures are the same in these configurations, see the next section.

The total power loss is a factor of 2 larger in the SXD1 than in the CD with no nitrogen, but as the CD detaches, similar power loss levels are achieved. The reduction of the peak plasma energy flux normal to the target between the CD and SXD1 increases throughout the scan from 5 (flux expansion) to ~ 100 (flux expansion plus power losses). The total power loss is similar in the SXD1 and SXD2 even at low nitrogen levels. What is affected by the additional poloidal flux expansion in SXD1 is the peak energy flux normal to the target which is reduced by approximately a factor of 2 compared to the SXD2.

3. Effect of divertor geometry on power exhaust in detaching plasma with nitrogen

Simulations with the target electron temperature close to 5 eV are selected from the scan in Fig. 2. For the CD, this corresponds to a puffing rate of 3×10^{22} N/s (nitrogen atoms per second), and for the SXD1 and SXD2 to a puffing rate of 4×10^{21} N/s. In these cases, plasma parameters in the divertor are more similar in all configurations than without impurity puffing (the case analyzed in detail in [4]). Fig. 3 shows the poloidal profiles of the temperature and density in all configurations. The temperature is constant along the poloidal coordinate in the upper SOL and sharply drops below the X-point. Tab. 1 gives a summary of plasma parameters in simulations both at around 5 eV and prior to seeding. We can see that before the nitrogen puffing, the target temperature in the SXD1 and SXD2 is reduced compared to the CD, mainly

as a result of larger target radius and cooling due to plasma-neutral interactions, and the same reduction is achieved in the SXD1 and SXD2. In the CD, both the inner and outer target detach as the puffing rate is increased (consistent with more radiation in the inner divertor and weaker closure with respect to neutral species), while the temperature at the inner target stays high in the SXD1 and SXD2 which have similar divertor closure properties (see Fig. 6 and related discussion). The effective charge at the core boundary is $Z_{\text{eff}} = 1.4$ in the CD and $Z_{\text{eff}} = 1.3$ in the SXD1 before the seeding, and increases to $Z_{\text{eff}} = 1.4$ in the CD and $Z_{\text{eff}} = 1.6$ in the SXD1 for the case around 5eV with maximum Z_{eff} on the grid reaching 1.9 in the CD and 3.5 in the SXD1.

Fig. 4 shows overall power balance in the simulations, with the power deposited at the targets and the power leaving the grid radially, the power loss divided into nitrogen ion radiation, carbon ion radiation, radiation from neutral species and additional losses caused to electrons and ions by interactions with neutrals. We can see that nitrogen ions radiate stronger in the SXD1 and SXD2 than in the CD in spite of lower puffing rates (larger radiation volume in the outer divertor, see later Fig. 5). In both SXD configurations, the power to the outer target is smaller, while the power to the inner target is larger. This is related to stronger radiation in the outer divertor, but weaker radiation in the inner divertor indicating there is less neutrals and impurities in the vicinity of the inner target. On the other hand, the neutral radiation and the additional losses are larger in the CD compared to the SXD cases, which will be discussed later in the paper. The total power loss is comparable in all configurations and reaches approximately 70% of the input power. It will be discussed in [6], that the total power loss and radiation saturate with increasing puffing rate after the detachment at approximately 80% of P_{inp} (similar maximum power loss in different configurations, but much higher impurity levels required in the CD to achieve this maximum).

The distribution of the power losses is shown in Fig. 5 separately for the radiation caused by carbon ions, nitrogen ions and neutral species. In the SXD1, the magnetic volume in the divertor is effectively used for nitrogen radiation along the whole length and the nitrogen radiation level is approximately twice larger than in the CD (Fig. 4). We can also notice a radial broadening of the nitrogen radiation in the flux-expanded region of the divertor, increasing the total nitrogen radiation level in the SXD1 with respect to the SXD2 by a factor of 1.2 (Fig. 4). The CD case leads to stronger nitrogen radiation in the inner leg (0.4% in the CD vs 0.1% in the SXD1), but on the other hand, the SXD cases achieve stronger nitrogen radiation in the outer part of the SOL, as well as in the core (0.5% in the CD vs 1.8% in the SXD1). The core radiation is, however, small compared to the power radiated in the outer divertor (9.1% in the CD vs 19.5% in the SXD1). Differences in the core radiation between the CD and SXD cases are likely caused by slight differences in the temperature distribution (Fig. 3). The distribution of impurity species (not discussed here) shows more neutral and ion impurity particles at low ionization stages in the inner divertor of the CD, and more impurity ions at higher ionization stages in the outer part of the SOL around the X-point in the SXD configurations. Concerning carbon radiation, the total level (7.8% in the CD vs 9.7% in the SXD1) as well as the power radiated above the X-point are comparable in the CD and SXD1 (note that in attached plasmas without seeded impurity, the differences in the power radiated by carbon are larger between the CD and SXD than reported here, and the SXD1 achieves better carbon impurity screening [4]).

The neutral radiation pattern shows that the inner divertor for the CD also radiates more in this component and there are more neutrals in the CD escaping the outer divertor and reaching the X-point and upper SOL. This is a combination of weaker divertor closure with respect to neutral species compared to the long baffled divertors (see later Fig. 6) and stronger recycling source at the target (Fig. 2). Apart from the radiation, Fig. 5 shows additional power losses

due to collisions with neutrals as it appears their contribution to the power loss is not negligible (Fig. 4), however it is not possible to separate different collision processes in this term in the simulation. We speculate that ionization processes make the key contribution in the CD and charge-exchange related losses are supposedly small as the temperature of neutrals at the target is comparable or even smaller than the plasma temperature in this case. Both the neutral radiation and the additional losses are stronger in the CD when integrated over the whole grid. This is because we are not comparing the CD and SXD configurations with the same operational parameters as for example in [4], but we assume that both configurations are close to detach. This requires much higher impurity puffing rate in the CD case. The CD then detaches with larger target particle flux (see Fig. 2) and larger recycling source resulting in stronger neutral-related power losses in this case.

Fig. 6 on the left shows the divertor closure with respect to deuterium atoms both prior and during the detachment. In the attached plasma without nitrogen, the closure in the SXD cases is dramatically improved compared to the CD (larger distance for neutrals to reach the X-point and shorter ionization mean free path due to lower temperatures and higher densities). Once the plasma is detached in both CD and SXD configurations, the advantage of the SXD cases over the CD is reduced because of similar temperatures in the divertor (Fig. 3) and more similar ionization mean free paths. On the right, the divertor closure with respect to nitrogen ion radiation is shown. While the SXD configurations radiate less in the inner divertor and inner SOL with respect to the CD, the level of the core radiation is slightly higher and is consistent with larger number of nitrogen particles in the core, likely related to differences in the temperature distribution. The divertor closure at the transition to detachment as calculated in Fig. 6 is therefore slightly weaker in the SXD cases than in the CD, but 92% of the radiation is still outside the core. The main effect is that in the CD, the divertor closure improves from the case (a) to (b)

where the radiation inside the divertor sharply rises with reduced temperature.

4. Conclusions

This paper follows from the work published in [4, 5] which showed that the modification of the divertor geometry in MAST-U to the SXD results in a high-recycling plasma compared to sheath-limited conditions in a standard divertor for the same upstream conditions. This was accompanied by an improved divertor closure with respect to neutral species and sputtered impurities, larger radiated power fractions and a strong reduction of the target power load. In this paper, we compare more alike divertor conditions in different magnetic configurations, which is achieved by different levels of impurity seeding. Three configurations are compared – a conventional divertor (CD), a Super-X divertor with large poloidal magnetic flux expansion (SXD1) and a Super-X divertor with small poloidal magnetic flux expansion (SXD2). The main aim is to investigate the effect of the magnetic geometry on the impurity radiation, the total power losses and the divertor closure.

Nitrogen puffing from the divertor chamber at large radius results in a stable detachment in the simulation with plasma radiating inside the divertor below the X-point. The SXD configurations require 7 times smaller puffing rate to detach than the CD, achieve larger pressure loss and faster reduction of the target power load, while keeping the target particle flux smaller as well. On the other hand, the inner target does not detach contrary to the CD where stronger radiation occurs in the inner divertor. Additional poloidal flux expansion in the SXD1 compared to the SXD2 reduces the peak target energy flux by a factor of 2, but does not reduce the target temperature and hence does not make the plasma detach earlier. Temperature levels in the SXD configurations are essentially set by larger target radius, which in these cases with strong baffling results in conditions where plasma-neutral interactions and radiation play more important role than the magnetic topology.

A detaching plasma in the SXD1 radiates approximately twice as much in nitrogen line radiation than in the CD and the nitrogen radiation is spread along the whole length of the divertor. Compared to the SXD2, the nitrogen radiation level is also slightly larger as the radiation pattern is broader in the flux-expanded region. On the other hand, the radiation from neutral species and an additional cooling attributed to processes such as ionization and charge-exchange are larger in the CD, which seems to be related to stronger recycling at larger puffing rate required for plasma detachment. Contrary to the nitrogen radiation, the radiation from neutrals is more localized around the targets and is stronger around the X-point in the CD compared to the long divertors. This indicates reduced divertor closure in the shorter leg, however, the advantage of the SXD cases over the CD becomes less significant in detachment compared to the case prior to seeding due to similar temperature levels once the plasma is detached. Regarding nitrogen radiation, the advantage of the SXD cases over the CD to screen impurities outside the core is similarly reduced during the detachment compared to the case before the detachment.

Acknowledgements

This work was funded by the RCUK Energy Programme [grant number EP/I501045] and by the European Union's Horizon 2020 research and innovation programme. The author gratefully acknowledges the support of X. Bonnin and D. Coster.

References

[1] P. M. Valanju et al., *Phys. Plasmas* **16**, 056110 (2009)

[2] G. Fishpool et al., *J. Nucl. Mater.* **438**, S356 (2013)

[3] W. Morris et al., *IEEE Trans. Plasma Sci.* **42**, 402 (2014)

[4] E. Havlíčková et al., *Plasma Phys. Control. Fusion* **56**, 075008 (2014)

[5] E. Havlíčková et al., *Contrib. Plasma Phys.* **54**, 448 (2014)

[6] (to be submitted 2014)

[7] V. Rozhansky et al., *Nucl. Fusion* **52**, 103017 (2012)

Figure captions

Figure 1. Three different connected double null configurations in MAST-U (CD in orange, SXD1 in black, SXD2 in blue). The impurity puff injector is located inside the divertor chamber (in magenta) and the cryopump behind the outer target (in green).

Figure 2. Transition to detachment in a nitrogen seeding scan in the outer divertor leg – (i) the peak parallel ion flux at the target, (ii) the peak parallel plasma energy flux at the target.

Figure 3. Poloidal profiles of the electron temperature and density at the separatrix between the outer midplane and outer target.

Figure 4. The power leaving the grid though boundaries and the power lost in the grid expressed in terms of the input power. $P_{\mathrm{t,out}}$ and $P_{\mathrm{t,in}}$ is the power to the outer and inner targets, P_{wall} is the power leaving the grid radially, $P_{\mathrm{loss,N}}$, $P_{\mathrm{loss,C}}$ and $P_{\mathrm{loss,neut}}$ is the power radiated by nitrogen ions, carbon ions and neutral species, $P_{\mathrm{loss,e}}$ and $P_{\mathrm{loss,i}}$ are additional losses caused to electrons and ions by other collision processes such as ionization and charge exchange. Note that $P_{\mathrm{loss,neut}}$ includes all neutral species – D, C, N, D_2.

Figure 5. The distribution of the power losses caused by different loss processes in three divertor configurations – CD (left), SXD1 (middle), SXD2 (right).

Figure 6. On the left, the divertor closure with respect to neutrals expressed as the ratio of the ionization source in the core and upper SOL and the ionization source in the whole grid. (a) is the case prior to nitrogen seeding, (b) is the case of a detaching plasma with different puffing

rate in different configurations. On the right, the divertor closure with respect to nitrogen ion radiation calculated as the ratio of the radiation in the core and the radiation in the whole grid. (a) is the case prior to detachment with the puffing rate 2×10^{21} , (b) is the case of a detaching plasma with different puffing rate in different configurations. Note that the result is only indicative as the radiation outside the grid and the radiation from nitrogen atoms can not be included in the calculation.

Table captions

Table 1. The electron temperature and density at the outer target $T_{\mathrm{e,t}}$ and $n_{\mathrm{e,t}}$, the electron temperature and density at the midplane $T_{\mathrm{e,sep}}$ and $n_{\mathrm{e,sep}}$, the electron temperature at the inner target $T_{\mathrm{e,in}}$. The temperature is in eV and the density in 10^{19} m^{-3}. The numbers in brackets are for the case prior to nitrogen seeding.

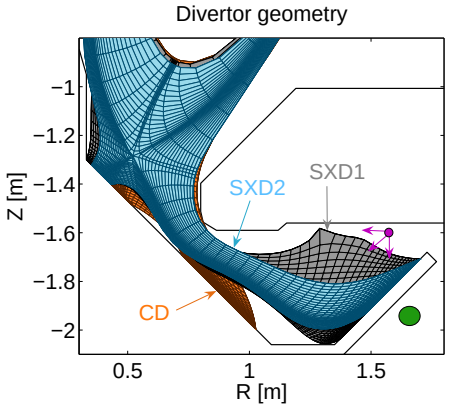

Figure 1

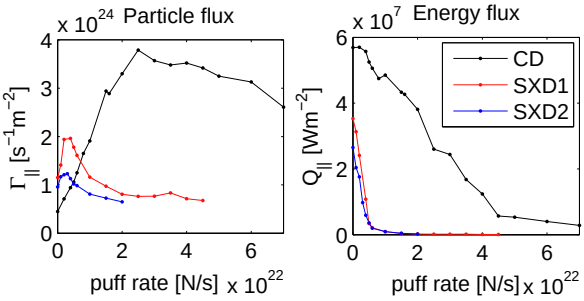
x 10^24 Particle flux
Γ_|| [s^-1 m^-2]
puff rate [N/s] x 10^22
x 10^7 Energy flux
Q_|| [Wm^-2]
CD
SXD1
SXD2
puff rate [N/s] x 10^22

Figure 2

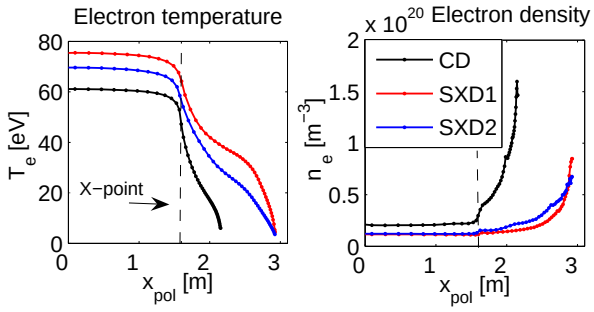
Electron temperature
80
60
40
20
0
T_e [eV]
X−point
0
1
2
3
x_pol [m]
x 10^20 Electron density
2
1.5
1
0.5
0
n_e [m^-3]
CD
SXD1
SXD2
0
1
2
3
x_pol [m]

Figure 3

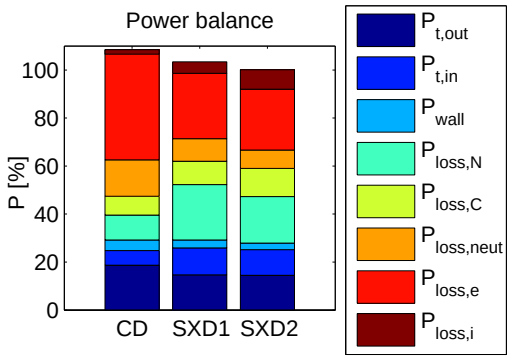
Power balance
P [%]
0
20
40
60
80
100
CD
SXD1
SXD2
P t,out
P t,in
P wall
P loss,N
P loss,C
P loss,neut
P loss,e
P loss,i

Figure 4

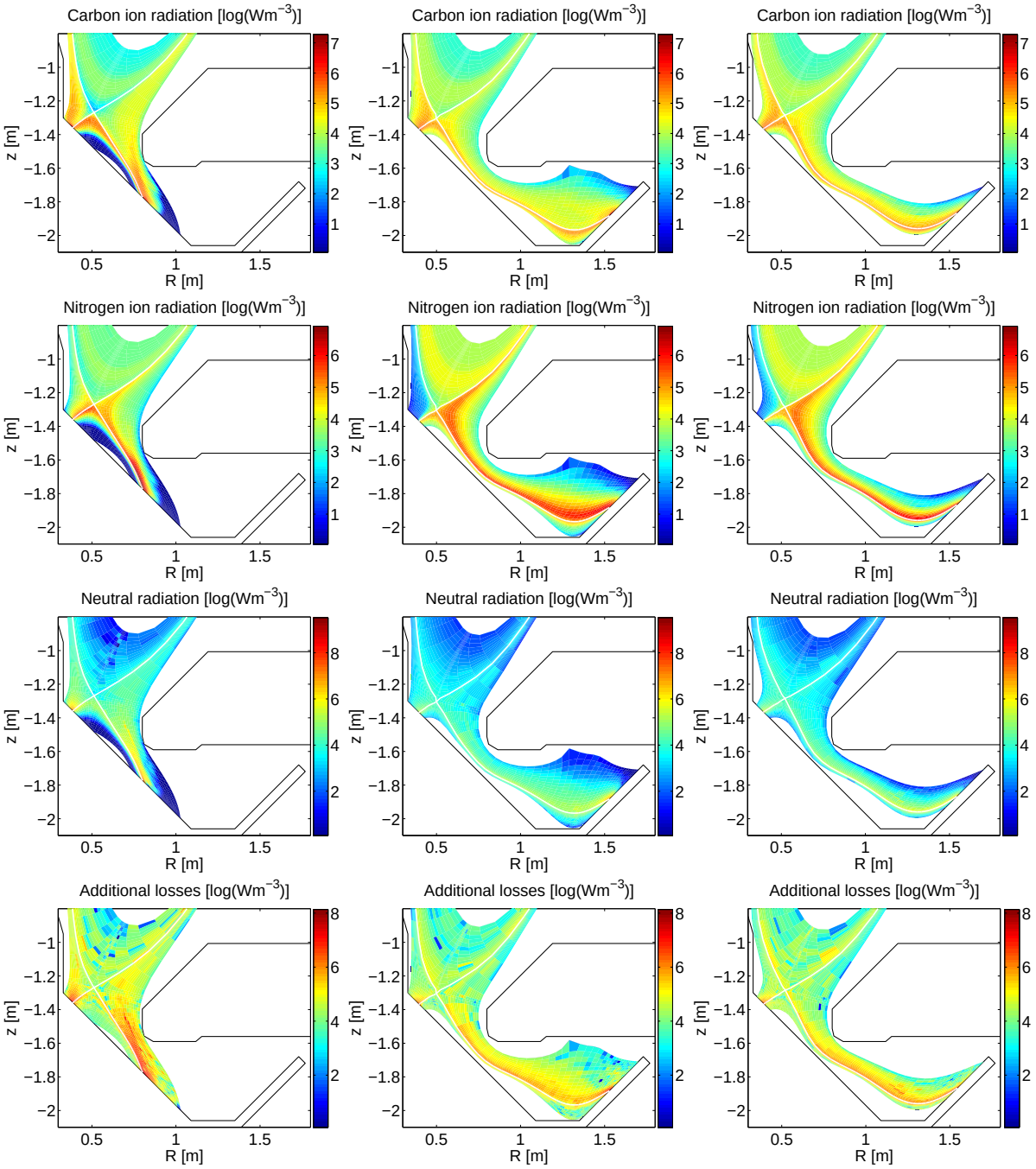
Carbon ion radiation [log(Wm^{-3})]
Carbon ion radiation [log(Wm^{-3})]
Carbon ion radiation [log(Wm^{-3})]
Nitrogen ion radiation [log(Wm^{-3})]
Nitrogen ion radiation [log(Wm^{-3})]
Nitrogen ion radiation [log(Wm^{-3})]
Neutral radiation [log(Wm^{-3})]
Neutral radiation [log(Wm^{-3})]
Neutral radiation [log(Wm^{-3})]
Additional losses [log(Wm^{-3})]
Additional losses [log(Wm^{-3})]
Additional losses [log(Wm^{-3})]
z [m]
R [m]

Figure 5

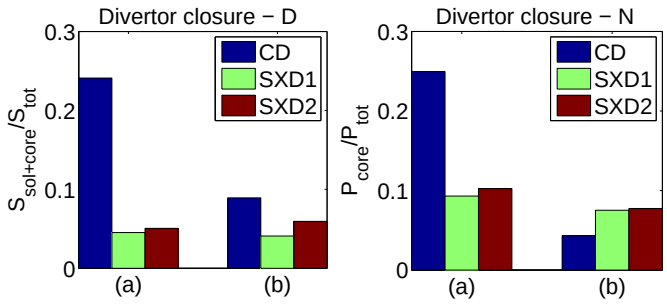
Divertor closure − D
Divertor closure − N
CD
SXD1
SXD2
$S_{sol+core}/S_{tot}$
P_{core}/P_{tot}
0.3
0.2
0.1
0
(a)
(b)

Figure 6

	$T_{\mathrm{e,t}}$	$n_{\mathrm{e,t}}$	$T_{\mathrm{e,sep}}$	$n_{\mathrm{e,sep}}$	$T_{\mathrm{e,in}}$
CD	6 (105)	24 (0.7)	61 (112)	2.0 (1.0)	5 (103)
SXD1	5 (30)	14 (3.2)	75 (81)	1.2 (1.0)	61 (72)
SXD2	4 (26)	7 (2.6)	70 (75)	1.2 (1.0)	50 (63)

Table 1